Electronic Supplementary Material (ESI) for Physical Chemistry Chemical Physics.
This journal is © the Owner Societies 2015

Supporting Information for:

Unassisted HI Photoelectrolysis Using n-WSe_2 Solar Absorbers

James R. McKone, Rebecca A. Potash, Francis J. DiSalvo, and Héctor D. Abruña*

Electrochemical cells

Two cells were used for photoelectrochemistry experiments—a single-chamber glass cell and a two-chamber acrylic cell. The glass cell consisted of a single large compartment with top-mounted ground-glass ports and a stopcock joint for gas purging. The bottom of the cell was made with flat optical-grade borosilicate glass, which gives good transmission of photons throughout the visible, near-IR, and near-UV wavelengths. Electrodes were placed near the bottom of the cell and illuminated from below as schematized in Figure S1. A rare-earth magnet attached to a small DC motor provided solution agitation via a PTFE-coated stir bar placed in the cell. Illumination was provided by a fiber-optic light source (Thorlabs OSL2), which was passed through a collimating optic, oriented horizontally, and reflected vertically using a silver mirror.

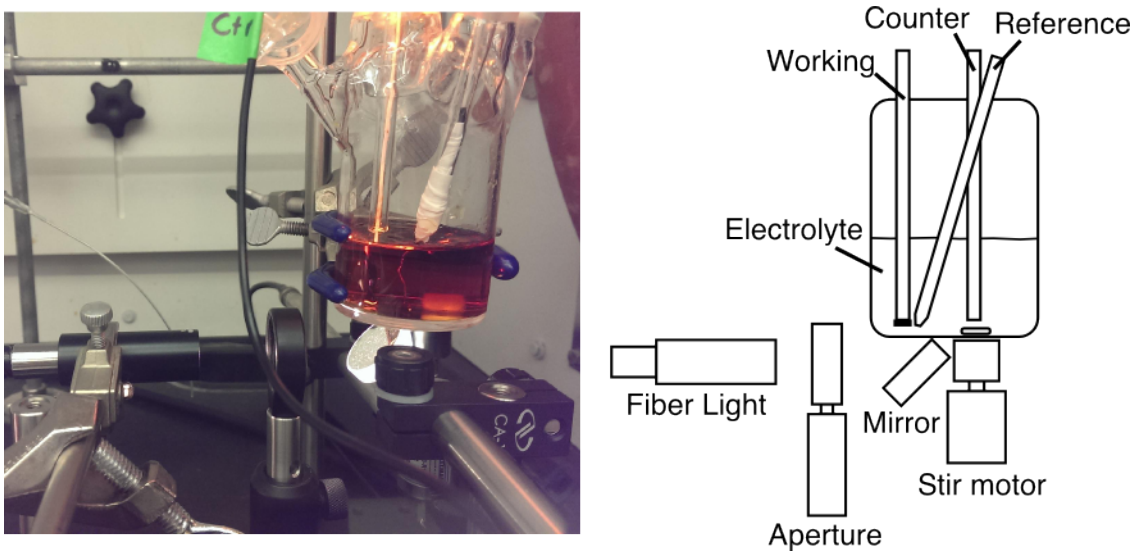

Figure S1. Photograph (left) and schematic (right) of the single-chamber glass photoelectrochemical cell.

The acrylic cell (schematized in Figure S2) consisted of two symmetric rectangular pieces with square compartments milled into each. Two such pieces were sandwiched together using a piece of Nafion® 117 as a gasket/separator and held together using four sets of screws and nuts. Holes were drilled in the top of each acrylic piece, allowing for electrolyte filling and insertion of electrodes. As with the glass cell, electrodes were oriented in a downward-facing fashion, and electrodes were also illuminated using the same approach. Solution agitation was provided by small stir bars driven by two DC motor/magnet assemblies, this time oriented horizontally so that the stir bars adhered to the sidewalls of the acrylic cell.

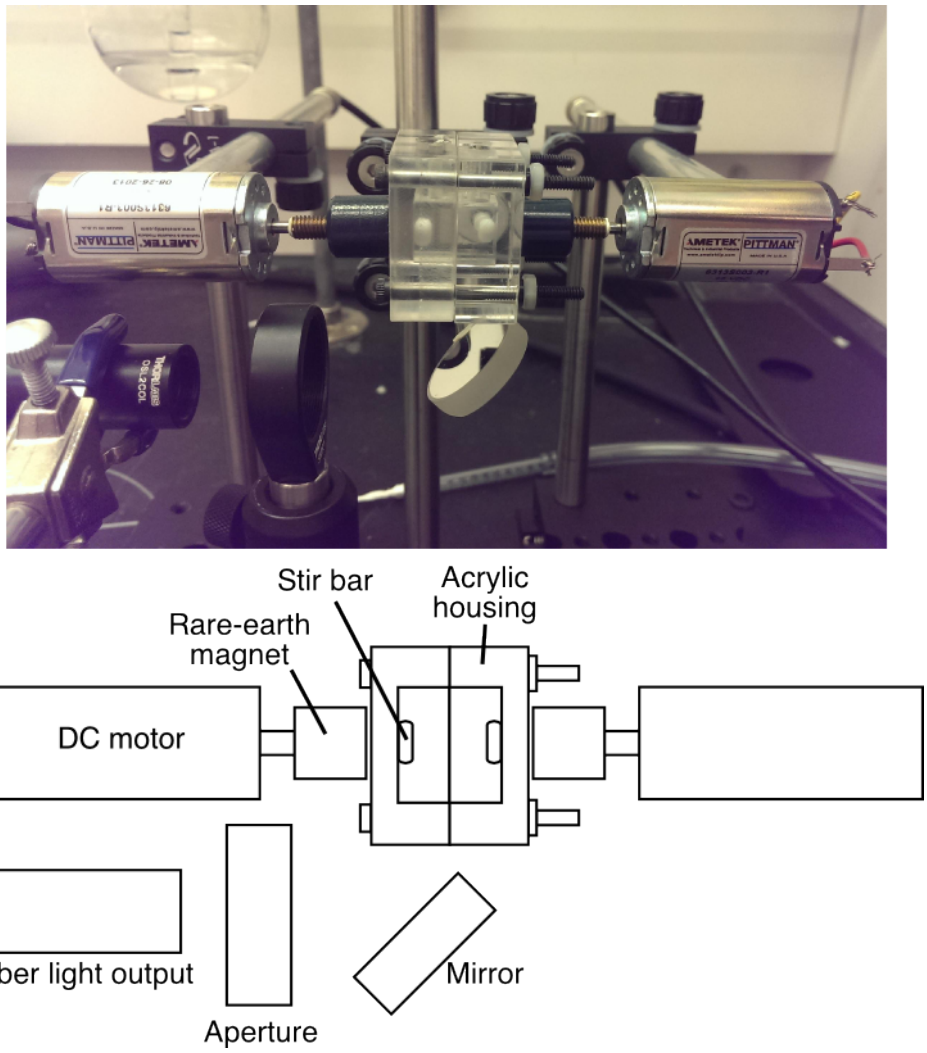

Figure S2. Photograph (above) and schematic (below) of the two-chamber acrylic cell.

Light source spectra and attenuation by iodide electrolyte

Figure S3(a)a shows the absorption spectrum of the aqueous triiodide ion. As noted in the main text, illumination of n-WSe_2 photoelectrodes was provided by a tungsten halogen light source. Figures S3(b) and (c) show, respectively, the AM1.5G and halogen lamp spectra before and after accounting for attenuation by a triiodide electrolyte at 5 mM concentration and a solution path length of 1 mm. The halogen lamp clearly provides a larger proportion of photons in the green and red wavelengths. As a result, the iodine-attenuated spectrum can facilitate a larger maximum photocurrent density than can the AM1.5 spectrum. This results in an overestimation of the energy-conversion efficiency for solar cells with bandgaps on the order of 1.1 eV, but the overestimate is not large enough to significantly alter the main conclusions of this study.

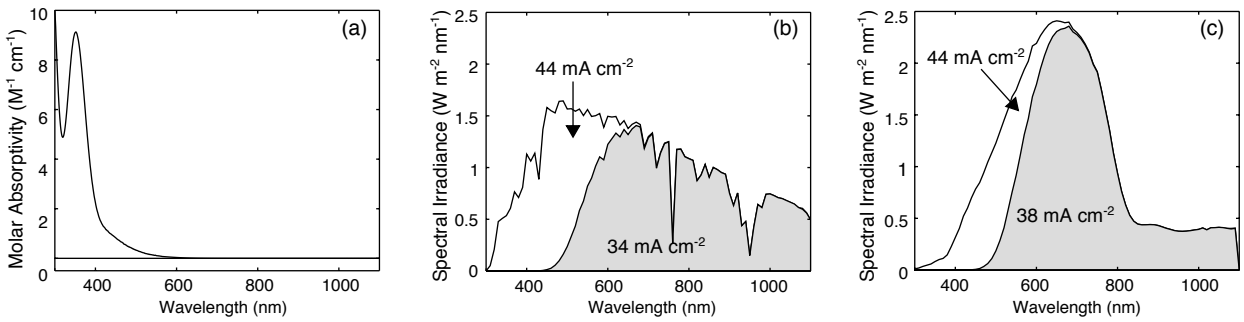

Figure S3. (a) Absorption spectrum of the triiodide ion collected using serial dilution of an aqueous HI electrolyte containing 0.1 M H_2SO_4, 0.1 M NaI, and 0.01 M I_2. Panels (b) and (c) contain full (shaded + unshaded) and attenuated (shaded only) spectra for the AM1.5 solar standard and an EKE-type tungsten halogen bulb. Attenuation was calculated from the absorbance spectrum in (a) using a triiodide concentration of 5 mM and a path length of 1 mm. The noted current densities correspond to the maximum that could be obtained for a solar cell assuming unity quantum efficiency across the spectra as shown.

Photoelectrochemical Figures of Merit

Tables S1 and S2 give the compiled figures of merit for all n-WSe_2 photoelectrodes used for this study operating in regenerative mode and energy-storage mode, respectively.

Table S1. Figures of merit for WSe_2 regenerative photoelectrochemistry

Sample	[HI] (M)	V_{oc} (V)	J_{sc} (mA cm^{-2})	FF	η_{HC} (%)	Notes
18-1	0.1	0.615	15.5	0.52	4.9	3-electrode
23-1	0.1	0.656	12.5	0.62	5.1	3-electrode
24-1	0.1	0.643	13.3	0.54	4.6	3-electrode
25-1	0.1	0.662	13.5	0.65	5.8	3-electrode
26-1	0.1	0.632	12.9	0.61	4.9	3-electrode
27-1	0.1	0.644	12.7	0.59	4.8	3-electrode
28-1	0.1	0.628	11.0	0.58	4.0	3-electrode
29-1	0.1	0.618	13.6	0.58	4.9	3-electrode
17-1	0.1	0.557	16.9	0.59	4.7	etched 3-electrode
18-2	0.1	0.564	11.3	0.53	3.4	etched 3-electrode
19-1	0.1	0.547	10.3	0.52	2.9	etched 3-electrode
21-1	0.1	0.554	6.5	0.55	2.0	etched 3-electrode
22-1	0.1	0.608	17.7	0.50	5.4	etched 3-electrode
28-3	0.1	0.632	13.9	0.53	4.6	etched 3-electrode
29-2	0.1	0.628	15.8	0.58	5.7	etched 3-electrode
26-2	0.1	0.63	13.7	0.69	5.2	2-electrode
27-2	0.1	0.644	13.0	0.59	5.0	2-electrode
28-2	0.1	0.625	10.4	0.59	3.9	2-electrode
23-2	1	0.653	13.3	0.61	5.3	3-electrode
25-2	1	0.653	13.3	0.60	5.2	3-electrode
27-3	1	0.641	12.8	0.60	4.9	3-electrode
28-4	1	0.572	13.5	0.57	4.4	3-electrode

Table S2. Figures of merit for WSe_2 HI photoelectrolysis

Sample	J_{op} (mA cm^{-2})	η_{FC} (%)
23-3	11.7	4.9
25-3	10.5	4.4
27-4	9.7	4.1
28-5	8.0	3.4

Concentrated HI stability measurement

Figure S4 shows the compiled results of a 21-hour stability measurement for an n-WSe_2 photoelectrode operating in regenerative mode in contact with 1.0 M HI electrolyte. Over the course of the experiment, the photocurrent diminished by 15% while the photovoltage decreased by <1 mV. Upon completion of the experiment, we observed that the electrolyte was darker in color. Using UV-visible absorption spectroscopy, we found that the electrolyte had indeed increased in triiodide concentration from ~1 mM to ~10 mM, leading to significantly greater light absorption in the 500-600 nm wavelength range. The darkening of the electrolyte can be attributed to slow air oxidation of iodide, which occurs readily in concentrated aqueous HI solution.

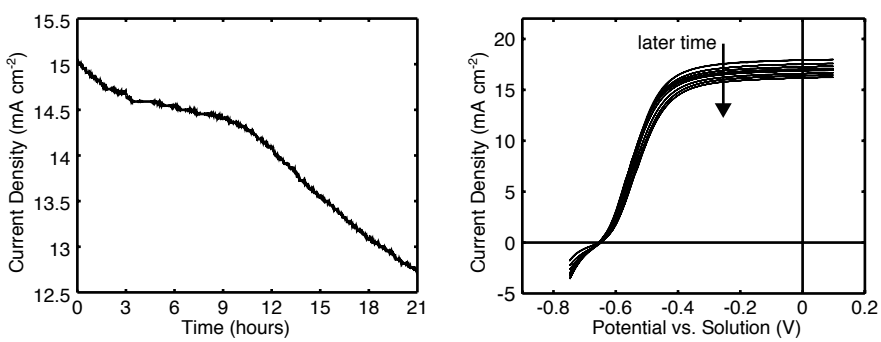

Figure S4. Potentiostatic measurements (left) and cyclic voltammograms (right) of an illuminated n-WSe_2 photoelectrode in 1.0 M HI electrolyte over the course of 21 hours. The potentiostatic measurements were collected in 3-hour intervals at -0.2 V versus the open-circuit potential of the photoelectrode. The voltammograms were collected every 3 hours, between potentiostatic measurements.

Mott-Schottky Methodology and Reproducibility

Mott-Schottky characterization was carried out on the basis of a simple Randles circuit model (Figure S5), where the parallel capacitance is taken as that of the semiconductor space-charge region. At appropriately high frequencies (usually in the range 1-50 kHz), the impedance is dominated by this space-charge capacitance, which can then be quantified by the simple relationship,

$$C_{\mathrm{SC}} = \frac{1}{2\pi f Z_{\mathrm{im}}} \tag{S1}$$

where f is the AC frequency and Z_{im} is the imaginary component of the impedance.

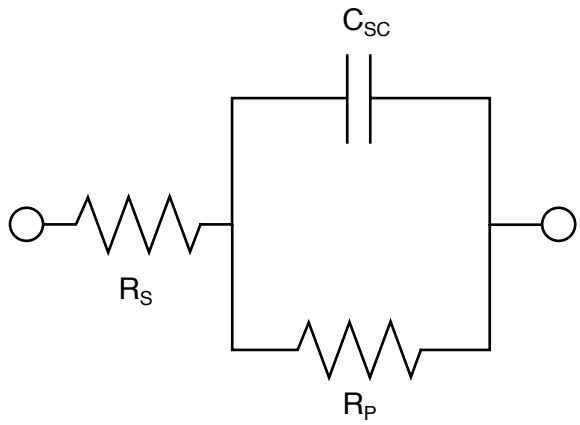

Figure S5. Schematic of the equivalent circuit used for M–S analysis.

For a crystalline semiconductor in contact with a kinetically facile redox couple, the above model is valid for applied potentials where the semiconductor is in reverse bias. In the case of n-WSe_2 in contact with an iodide electrolyte, the reverse bias condition is satisfied for potentials positive of ~0.3 V versus Ag/AgCl. We independently determined that oxidation of the WSe_2 crystal begins at potentials near the reversible oxygen electrode potential, or ~1 V vs Ag/AgCl. Thus we chose to measure capacitance over a range of DC bias from 0.0-0.9 V vs Ag/AgCl.

We explicitly confirmed that the response was capacitive by ensuring that the phase angle of the frequency response was between -85 and -90 °. We found this generally to be true for n-WSe_2 electrodes using a 10 mV AC oscillation at 5 kHz. Thus, the data were collected under these conditions and the resulting M–S data were fit over the reverse-bias potential range of 0.4-0.8 V vs. Ag/AgCl. This procedure generally yielded good linear fits and n-type doping densities of $5 \pm 1 \times 10^{16}$ cm^{-3}, which agrees well with the observed photoelectrochemical behavior. Note that extending the fits over the full range of 0.3-0.9 V decreases the quality of the linear fit, but it does not significantly alter the primary results and conclusion of the measurements.

The relationships between capacitance and the relevant semiconductor parameters are as follows:

$$\frac{1}{{C_{\mathrm{SC}}}^2} = \frac{2}{\varepsilon\varepsilon_0 A^2 e N_{\mathrm{D}}}\left(V - V_{\mathrm{fb}} - \frac{kT}{q}\right) \tag{S2}$$

where C_{SC} is the space-charge capacitance, ε is the relative permittivity of the semiconductor (4.5 for WSe_2), ε_0 is the vacuum permittivity, A is the semiconductor active area, e is the signed fundamental electronic charge, N_D is the semiconductor doping density, V is the applied potential, V_{fb} is the flatband potential, k is the Boltzmann constant, T is the temperature, and q is the unsigned fundamental electronic charge. This expression can be rearranged to

$$\frac{\varepsilon\varepsilon_0 A^2 e}{2{C_{\mathrm{SC}}}^2} \approx \frac{1}{N_{\mathrm{D}}}(V - V_{\mathrm{fb}}) \tag{S3}$$

where the Boltzmann factor has been omitted since at room temperature it is small relative to the applied potential. The left side of this equation collects all of the relevant constants, along with the space-charge capacitance measured by impedance spectroscopy, and can be expressed as a M–S parameters in units of $cm^3 \cdot V$. A plot of this M–S parameter versus the applied potential will have a slope equal to the inverse of the doping density and an x-intercept equal to the flatband potential (within a factor of kT).

Figure S6 shows three Mott–Shottky datasets that were collected on separate n-WSe_2 photoelectrode samples from the same crystal growth run. The extrapolated flatband potential varied over ~0.05 V, and the doping density implied from the slopes of the lines varied from 3.3–6.0 x 10^{16} cm^{-3}. In general, doping densities for all samples tested in various electrolytes varied over a similar range, while standard deviations in the measured flatband potentials are captured in the error bars in the main text Figure 7b. We conjecture that variable surface step-edge density for the n-WSe_2 photoelectrodes could be responsible for increased spread in measured flat-band potentials at high iodide concentrations due to different electronic effects of iodide adsorbed at step edges versus basal planes.

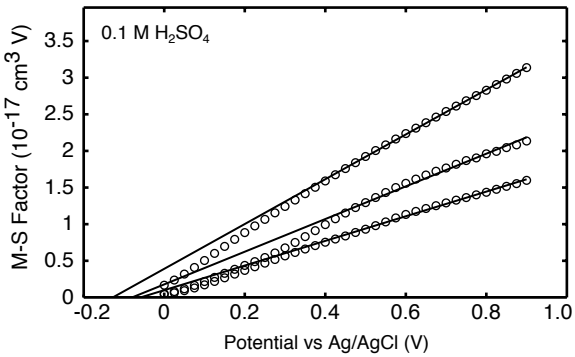

Figure S6. Mott–Schottky data for three different n-WSe_2 electrodes collected in 0.1 M H_2SO_4 elecrolyte without addition of sodium iodide.